FULL PAPER

# Charge Generation at Polymer/Metal Oxide Interface: from Molecular Scale Dynamics to Mesoscopic Effects

*Ajay Ram Srimath Kandada, Simone Guarnera, Francesco Tassone, Guglielmo Lanzani, and Annamaria Petrozza**

**The correlation between molecular scale morphology and charge generation across hybrid photovoltaic interfaces made of metal oxides (ZnO and $TiO_2$) and a prototypical electron donor polymer, P3HT, is investigated. Device characterization and UV-NIR transient absorption spectroscopy are used to demonstrate that the local disorder of the polymer chains on the surface of the metal–oxide film provides better electron injection efficiencies than the crystalline phases, though the latter are essential for energy and charge transport. An unambiguous spectroscopic tool is also demonstrated to probe the occupation of the conduction band of ZnO following the electron injection from the polymer through the ultrafast tracking of the Burstein-Moss effect.**

## 1. Introduction

Substitution of fullerene molecules with metal oxide nanostructures in polymer based solar cells is expected to provide many superior characteristics such as high dielectric constant that facilitates exciton dissociation, greater carrier mobility for efficient charge collection and good morphological and thermal stabilities.[1–4] In spite of such expected advantages, polymer based hybrid solar cells have not shown decent performances, with the best devices giving 2% power conversion efficiency in BHJ[3] architecture and 0.1% in the bilayer design. These values are much lower in comparison with the all-organic BHJ solar cells[5] suggesting other optoelectronic mechanisms are playing a role. Recently, interface engineering in polymer/metal-oxide solar cells has been exploited in order to enhance the device performances.[3,6–9] Attention was on a) energy level alignment of the electron donor and acceptor compounds[10] and b) control of the interface morphology.[6] In the first case no actual improvement could be demonstrated in the overall power conversion efficiency of the device due to a tradeoff between the short circuit and the open circuit values. In the second case, it was found that a good level of crystallization both of the organic and inorganic part seems to play a role.[6,7] All this calls for a detailed understanding of the microscopic dynamics at the interface. In particular, to what extent the interface morphology and the local crystallinity affect the efficiency of charge pair generation is unknown. Time resolved spectroscopy is in general a very fruitful tool for studying the dynamics. However, because the photoexcitation is a bulk process there is an unavoidable overlap of interface and bulk response in most spectroscopic data. One of the major challenges is thus the disentangling of the overwhelming bulk polymer contribution from the interface contribution. Till now, electron injection rates have been extracted from complex modeling of the femtosecond transient absorption data.[11] Those are essentially based on polymer spectroscopic features that are not interface-specific. In addition looking at polymer features does not provide any information on the final state of injection.

In this work, we study the effect of local morphology on the charge generation dynamics in proto-typical hybrid interfaces of compact metal-oxide films (zinc oxide (ZnO) and titanium dioxide ($TiO_2$), electron acceptors with a large technological interest) with poly 3-hexyl thiophene (P3HT). The latter allows us to tune the polymer interface morphology from amorphous to crystalline. We directly monitor charge injection into the oxide by tracking the Burstein-Moss shift of the band-edge using 150 fs transient absorption (TA) spectroscopy. This technique is sensitive to the conduction band occupation in the oxide semiconductor. Thus, it provides an unambiguous fingerprint of the charge transfer at the interface to a site where they can effectively be transported, in contrast with electron transfer to trap states. Combining the spectroscopic data with those on device parameters, we assess the role of disorder in charge generation across the interface.

## 2. Results and Discussion

**Figure 1**a shows the absorption spectrum of regio-regular(rr) and regio-random(rra) P3HT films deposited on quartz, along with the absorption spectrum of a rr-P3HT film coated on 200 nm thick mesoporous $TiO_2$ substrate. The latter generally corresponds to the partial filling of the mesoporous structure

Dr. A. R. S. Kandada, S. Guarnera, Dr. F. Tassone, Prof. G. Lanzani, Dr. A. Petrozza
Center for Nano Science and Technology @ PoliMi
Istituto Italiano di Tecnologia
via Pascoli 70/3, 20133 Milano, Italy
E-mail: annamaria.petrozza@iit.it
S. Guarnera, Prof. G. Lanzani
Dipartimento di Fisica
Piazza Leonardo da Vinci 32
20133 Milano, Italy

DOI: 10.1002/adfm.201303689

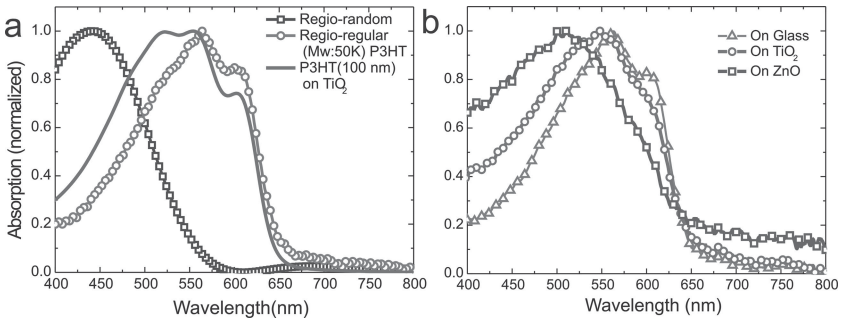


**Figure 1.** a) Absorption spectra of rr-P3HT, rra-P3HT on glass and 100 nm film spin coated on mesoporous titania. b) Normalized absorption spectra of rr-P3HT film of <5 nm thickness spin coated on glass, $TiO_2$ and ZnO.

together with a pure P3HT capping layer. The $TiO_2$/P3HT composite spectrum mainly resembles the rr-P3HT absorption spectrum. Figure 1b shows the absorption spectra of <5 nm thick rr-P3HT film on glass, $TiO_2$ and ZnO compact layers. Moving from quartz, to $TiO_2$ and ZnO, there is a blue shift in the absorption spectrum of extremely thin films of rr-P3HT, tending towards the absorption of rra-P3HT. It was shown by Spano and co-workers that the 0–0 vibronic peak is extremely sensitive to the environment as well as to the exciton bandwidth (and hence the extent of aggregation).[12,13] In the case of amorphous phase of the polymer, the vibronic peaks are quenched accompanied by a blue shift of the absorption band edge (Figure 1a, rra-P3HT). On the other hand, a crystalline phase with parallel stacking of the chains shows clear vibronic peaks with a red shifted absorption band (Figure 1a, rr-P3HT). It has been previously suggested through molecular dynamic calculations that the physisorptive interaction of the polymer with the metal-oxide and the consequent thermodynamical effects can significantly alter local morphology of the polymer.[6,14] Since the morphology has a direct consequence on the absorption spectrum,[13] we thus get clear experimental insight on our samples. Close to the oxide interface the polymer phase is mainly disordered, while, getting away from it, that is, in the bulk of the sample, the P3HT chains start packing in an orderly fashion.

**Figure 2** illustrates characterization of bilayer devices made with compact layers of metal–oxide with >50 nm film of P3HT spin coated on top. The devices architecture is not optimized for delivering high performances solar cells, however, it helps us to spot the influence of interface processes at a macroscopic level. Figure 2a shows the figures of merit (open circuit voltage ($V_{oc}$), short circuit current ($J_{sc}$), fill factor (FF), and efficiency ($\eta$)) for a set of devices made with ZnO and $TiO_2$. ZnO devices show superior performances with respect to those of $TiO_2$. While the $V_{oc}$ values are very similar, the $J_{sc}$ drives the improvement. Figure 2b,c show normalized external quantum efficiency spectra compared with absorption spectra (percentage of absorbed light) of the bilayer devices with $TiO_2$ and ZnO respectively. Interestingly the EQE in both the cases has predominant contribution from the blue part of the absorption spectra of the polymer showing that photocurrent mainly comes from the photoexcitation of the amorphous domains of the polymer, the blue part of the spectrum. This goes against the common notion that it is the crystalline phase the one required for efficient device performance. It is also intriguing to see that ZnO devices which have larger amorphous interface morphology show higher photocurrent and efficiency with respect to $TiO_2$, at comparable $V_{oc}$ values.

**Figure 3**a,b show the femtosecond transient absorption spectra of the bilayers comprising of ≈200 nm ZnO and <50 nm of rr-P3HT or rra-P3HT spin coated on top. The pump wavelength is at 540 nm. In the spectral range between 450 nm and 650 nm both samples show a positive band ($\Delta T/T > 0$) attributed to the polymer ground state bleach (GSB) (see Supporting Information, Figure S2 for the complete set of TA kinetics in the VIS-NIR spectral region). TA in the UV spectral region has two main features: a positive band corresponding to the absorption edge of ZnO at 365 nm and a photo-induced absorption band (PA) at 345 nm. The absorption spectrum of ZnO substrate is shown in Figure 3c along with its first derivative. The positive feature spectrally overlaps with the first derivative of the absorption spectrum. Because there are no TA bands belonging to P3HT in this spectral region (TA spectra at these probe wavelengths of rr-P3HT and bare ZnO are given in the Supporting Information, Figure S3) the positive peak at 365 nm should stem from the blue shift of the band edge of ZnO. We assign this

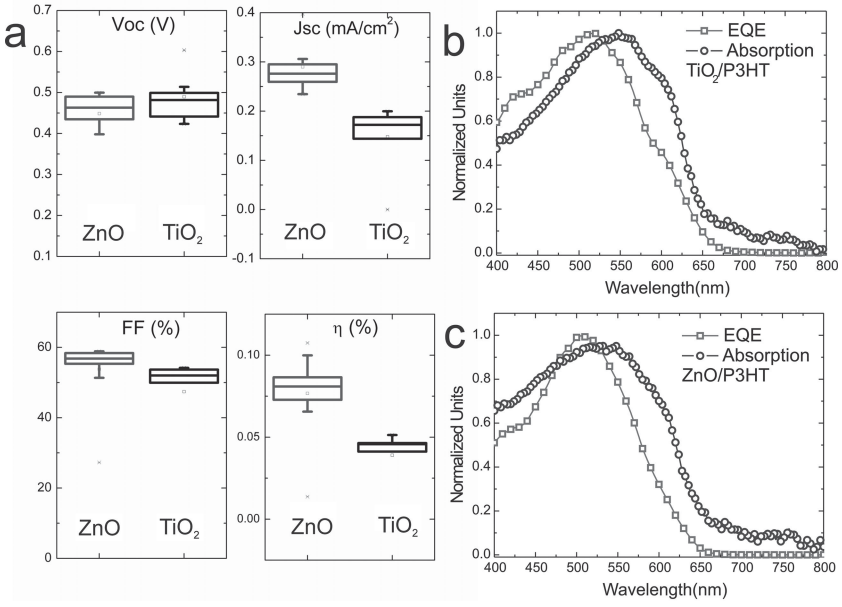


**Figure 2.** a) Device characteristics of bilayer devices made of ZnO or $TiO_2$ and 50 nm of rr-P3HT. b,c) Normalized EQE spectra of $TiO_2$ and ZnO devices plotted along with the absorption (percentage of absorbed light) spectra.

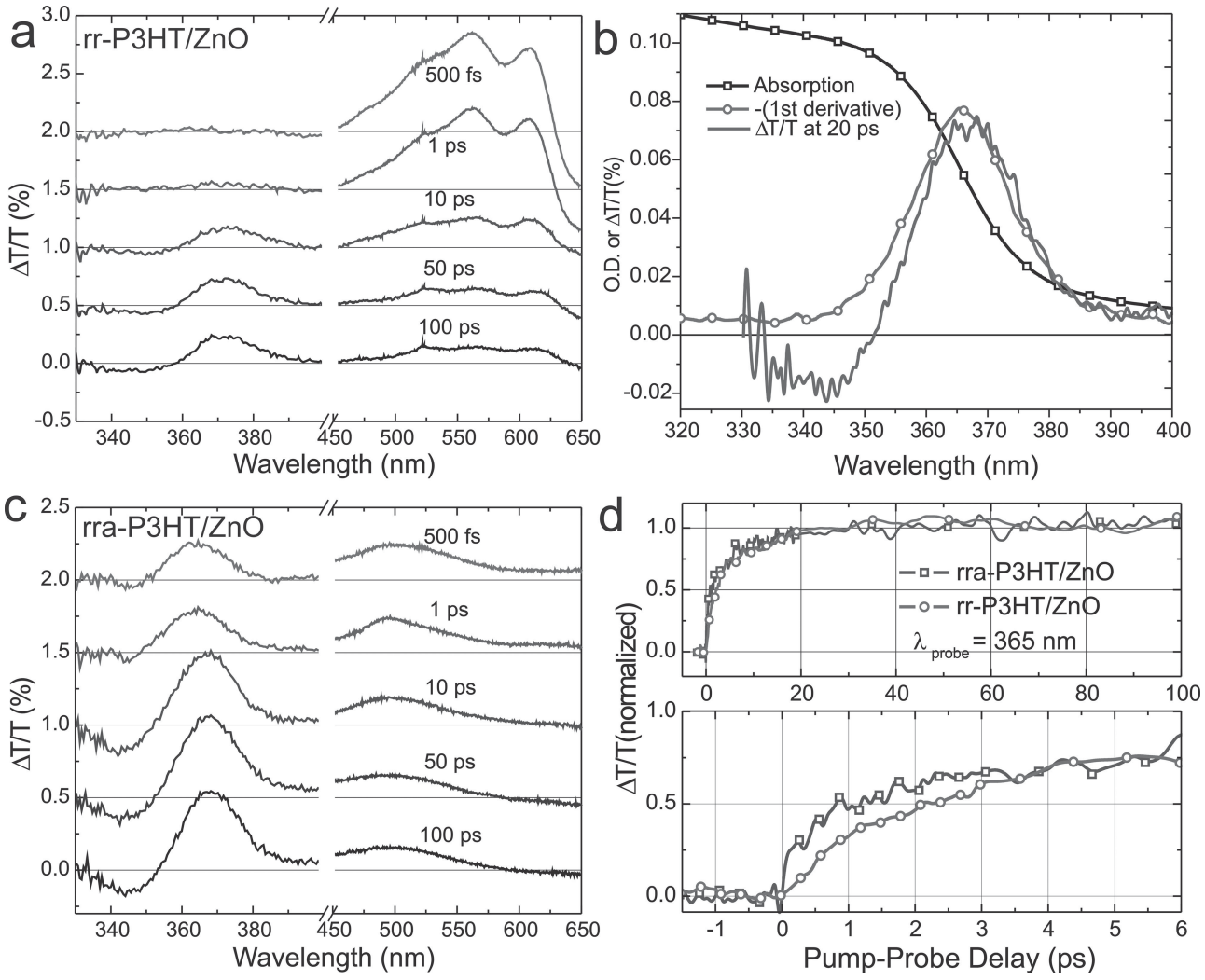


**Figure 3.** a) Transient absorption spectra of ZnO/rr-P3HT (<50 nm) bilayer. The pump pulse at 540 nm is used with an excitation density of $2 \times 10^{18}$ $cm^{-3}$. b) Absorption Spectrum of ZnO along with its first derivative. Also overlapped is the TA spectrum of ZnO/P3HT bilayer. c) TA spectra of ZnO/rra-P3HT bilayer; pump at 500 nm with similar excitation density as the previous case. d) Normalized TA kinetics at l $\lambda_{probe}$ = 365 nm for rr and rra P3HT on ZnO.

blue shift to the Burstein- Moss effect[15] due to the electron injection from photoexcited P3HT into the conduction band of ZnO. Filling of the lowest states in the ZnO conduction band causes a blue shift of the optical gap[16–18] due to Pauli blocking of the electronic transitions reaching those states. To corroborate our assignment we note that similar changes in the absorption spectra are observed by exposing the ZnO susbstrates to UV light for about 30 min in vacuum (see Supporting Information, Figure S4), as a consequence of photo-doping.[19,20] We conclude that the kinetics measured at $\lambda_{probe}$ = 365 nm selectively probes the electron population in the conduction band of ZnO, and thus the electron transfer dynamics. This direct access to the phenomenon is a distinct advantage in our approach, as so far injection dynamics have been inferred only indirectly by the numerical analysis of the complex lineshape of the transient spectra.[6,11]

The UV feature appears immediately upon photoexcitation when rra-P3HT is interfaced with the oxide (Figure 3c). On the contrary in presence of rr-P3HT, electron population in ZnO builds up in the first 300fs, while the polymer PB band decays, indicating the concomitant loss of population (see Figure 3d for the UV features dynamics). Moreover, when disorder is induced in the rr-P3HT phase, upon treatment of the ZnO substrate, the injection rate becomes faster (see Figure S5 in the Supporting Information).

Exploiting the probing of the Burstein shift we can get quantitative information on the charge injection as a function of different polymer morphologies. In degenerate semiconductors it is directly related to the carrier density in the conduction band by the relation[21]

$$\Delta E_{\text{Burstein}} = \frac{h^2 N_{\text{CB}}^{2/3}}{8 m_e^* \pi^{2/3}} \quad (1)$$

$N_{\text{CB}}$ represents the carrier density in the conduction band injected from the polymer, $m_e^*$ is the effective mass of electron,

which is around 0.35 $m_e$ in ZnO[19] and $h$ is the Planck's constant. The measured Burstein shift ($\Delta E_{Burstein}$) can hence be associated to the injected carrier density ($N_{CB}$). In the case of rr-P3HT/ZnO interface, we observe $\Delta E_{Burstein}$ of approximately 1 meV, that corresponds to $N_{CB}$ of $4.5 \times 10^{16}$ cm$^{-3}$. For a similar excitation density, in the case of rra-P3HT/ZnO interface, we observe $\Delta E_{Burstein}$ of 5 meV and a corresponding $N_{CB}$ of $4.9 \times 10^{17}$ cm$^{-3}$. This simple calculation shows that injection efficiency, approximated as the ratio between the injected carrier density and excitation density, is roughly one order of magnitude higher in the case of rra-P3HT.

In general, population of the conduction band in a semiconductor give rise to two simultaneous and competing effects: a) state filling and Pauli blocking leading to blue shift of the optical gap, the Burstein shift (BS) and b) band gap renormalization (BGR)[21–24] leading to the shrinkage of the gap. Usually in heavily doped systems such as ZnO (n doped),[25] BS overtakes BGR.[22] Hence, Equation 1 is a valid approximation that probably under-estimates the injected carrier density. This inaccuracy however does not alter the statement on the relatively higher injection efficiency in the case of rra-P3HT. Finally, the PA at 345 nm can be tentatively assigned to absorption of a Mahan exciton.[23] Briefly, injection of electrons into the CB brings about an additional screening of the electron-hole interaction that eventually leads to the Mott transition. Such a transition is preceded by the formation of a Mahan exciton-a multi particle bound state resulting from the interaction of the excited electron-hole pair with the Fermi sea.[22,23] As a result of this interaction, the oscillator strength at the absorption edge is enhanced. We believe that this accounts for the appearance of a PA band at 345 nm upon injection of a large density of carriers.

Effective atomic passivation of the surface traps on the metal-oxide can also be seen as a reason for improved injection from the disordered polymer. However, recent studies of such an interface show no evidence of passivation or a chemical interaction between the polymer and the metal-oxide surface.[14,26] Hence our results highlight the role played by local morphology specifically onto the polymer/oxide coupling, and suggest that injection from the amorphous polymer phase is more efficient than from the polymer aggregate. This does not however provide a simple formula for the optimum device, because the device performance is actually given by the trade-off between injection and transport.

An enhancement of the device efficiency has been previously reported due to the surface treatment of the mesoporsous $TiO_2$ layer with mercapto pyridine.[6] However, a more ordered polymer packing was predicted at the interface. This can be directly inferred from **Figure 4**a which shows the appearance of vibronic peaks in the absorption spectrum of 5 nm RR-P3HT spin coated on top of the treated compact $TiO_2$ susbtrate. Greater order should quench the injection efficiency. In fact the bilayer devices show inferior performance with such a treatment (Figure 4b). The order phase favors energy transport to the interface and charge separation off the interface, but not necessarily the charge injection. Thus, morphology plays opposite roles, and the optimum is given by the interplay between local coupling and local transport, of charge and energy.

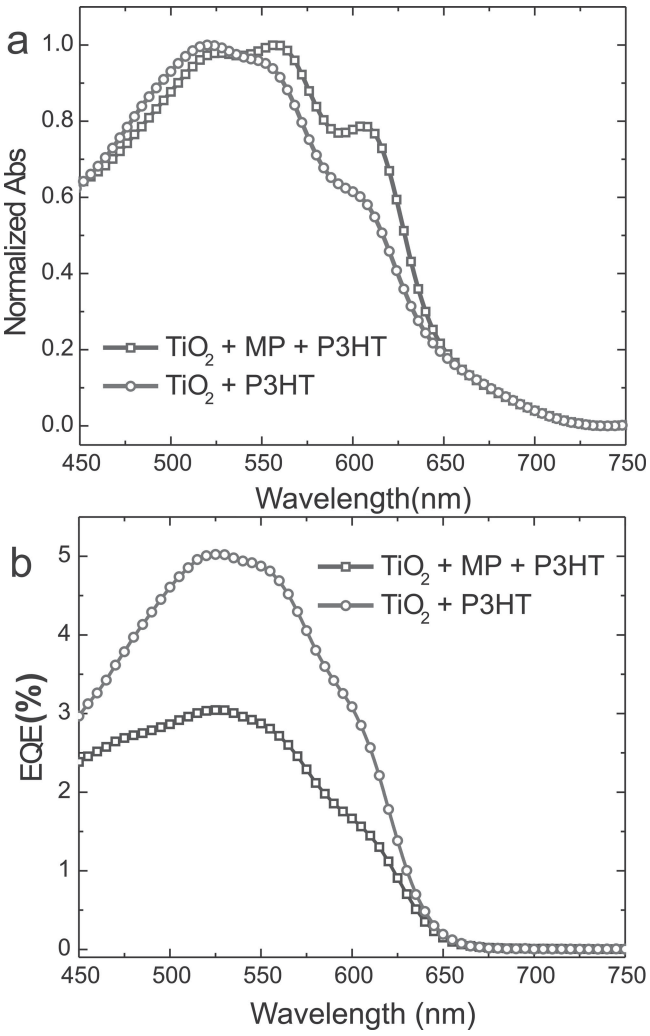


**Figure 4.** a) Normalized absorption spectra of <5 nm rr-P3HT on untreated and mercapto-treated $TiO_2$ susbtrates. b) External quantum efficiency spectra of devices with treated and untreated titania.

It is worth noting that the dynamics in Figure 3d show that the electron injection process is completed in less than 20 ps irrespective of the local morphology at interface. Such a time scale points to null or minimum contribution from exciton diffusion. We prove this by comparing transient dynamics following the excitation from either the polymer or the ZnO side, that is, the polymer bulk or the interface, respectively. Accordingly, in both excitation geometries we measure the same injection rate (**Figure 5**). There is however a difference in signal intensity at 365 nm in the two cases even after proper normalization for the excitation density, showing in particular larger injection for the interface excitation case. This allows us to conclude that excitons close to the interface contribute to the photocurrent and the rest of them are wasted. This can be explained by the observation that the disordered phase has a larger optical gap than the rr-phase, due to both chain conformation and inter chain coupling. The energy mismatch is unfavorable for Förster like energy transfer[27,28] between the two phases, and it acts as a barrier to energy harvesting from the bulk. In spite of

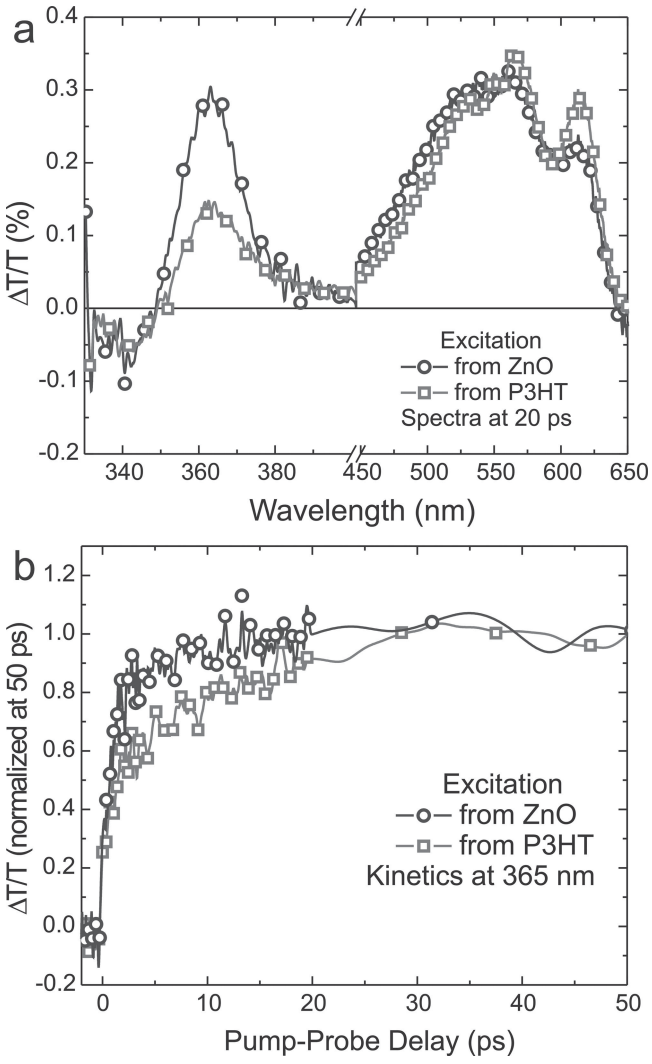


**Figure 5.** a) TA spectra taken at 20 ps pump-probe delay of rr-P3HT/ZnO sample collected with excitation from the ZnO side and from the side of the polymer. This corresponds to direct interface excitation and bulk excitation respectively. b) Associated normalized TA kinetics at the probe wavelength at 365 nm.

a better energy transport in the crystalline phase, energy stops near the interface. Even though there is a need to have large domains of crystalline P3HT for an efficient extraction of free charge carriers, the intrinsic disorder at the hybrid interface hinder the harvesting of most of the photo-excitation that goes into the aggregates as evident from the EQE spectra.

It must be noticed that local disorder in the polymeric phase has been reported also at fully organic interfaces, that is, P3HT:PCBM.[29] However, it has never been associated to a limitation in exciton harvesting at the interface. This is consistent with an ultra-fast energy transfer mechanism found as primary process at the donor/acceptor interface[30] which allows to overcome such a problem. Of course there is no chance to have energy transfer in the presence of high band gap electron acceptor semiconductors like $TiO_2$ and ZnO, which leads to unavoidable low performances of the photovoltaic device.

## 3. Conclusions

This work shines light onto the relationship between the local morphology and the electron injection dynamics in polymer/oxide interfaces for photovoltaics. It also introduces a photo physical tool for monitoring interface dynamics in hybrid organic/oxide interfaces. The Burstein shift of the oxide optical band-edge is used as a selective probe for the electron population in the conduction band. This allows us to measure in a direct way, the electron injection from the polymer after photoexcitation, and to identify the important parameters ruling it. Reported data allows disentangling the interface coupling from the transport issue. We find that local disorder of the polymer chains at the surface of the oxide provide better efficiency of electron injection than ordered aggregate or crystallite. The improved injection in the amorphous polymer phase is however hard to be exploited in devices, for transport is worse with respect to the crystalline phase.

## 4. Experimental Section

*Sample Preparation*: ZnO films are prepared by sol-gel technique as described by Sun et al.[31] 1 gm of zinc acetate dihydrate(Sigma Aldrich, 99.999%) is dissolved in 10 mL of 2-methoxyethanol (Sigma Aldrich, 99.5%) and 0.28 g of ethanolamine (Sigma Aldrich, 99.0%). The resulting solution is stirred overnight at room temperature in air. Thin films of ZnO are prepared by spin-coating the solution on quartz substrates at 1500 rpm for 60 s and finally dried at 150 °C for 1 h in air. $TiO_2$ compact layers are deposited by spray-pyrolysis. The deposition is carried on starting from a 1:10 by volume titanium diisopropoxide bis(acetylacetonate):ethanol (Sigma Aldrich) solution with oxygen as carrier gas. During the spray-pyrolysis process the substrates are placed on a hot-plate at 400 °C. Finally they are annealed at 500 °C for 30 min. P3HT (Merck, Mw = 80 000) is then spin-coated on the substrates starting from solutions in chlorobenzene with concentrations spanning from 1 mg $mL^{-1}$ to 30 mg $mL^{-1}$ depending on the desired thickness. For electrical characterization, on top of the substrates a thin (≈60 nm) layer of silver is evaporated.

*Device Characterization*: Current–voltage characteristics of the solar cells are measured by a Keithley 2440 Source Meter under 1 sun illumination (AM1.5) provided by a solar simulator (Oriel class AAA, Newport).The external quantum efficiency (EQE) measurement is carried out by using a quartz tungsten halogen lamp (Newport) coupled to a monochromator (Oriel CornerstoneTM 260 1/4 m).

*Transient Absorption Spectroscopy*: Pump pulses centered at 540 nm are generated from a home built noncollinear optical parametric amplifier starting from a Quantronix laser system (1 W, 1 KHz repetition rate, 150 fs pulse duration, 800 nm wavelength). The probe pulses in the UV-Vis region is generated by focusing 2 μJ of the laser fundamental on a 5 mm thick $CaF_2$ crystal. To avoid damaging the crystal due to high laser fluence, it is constantly moved using motorized XZ stages. Pump-Probe setup employing a computer controlled optical multichannel analyzer enabling single-shot detection at 1 KHz repetition rate is used to measure the normalized transmission change, $\Delta T/T$. Pump pulses are focused at the sample in a 200 μm diameter spot with excitation energy of about 30 nJ per pulse. All the measurements are done at room temperature and in vacuum.

## Supporting Information

Supporting Information is available from the Wiley Online Library or from the author.

## Acknowledgements

The authors would like to thank Prof. G. Cerullo and Dr. F. Scotognella for useful discussions and help with the experimental setup.

Received: October 30, 2013
Revised: December 7, 2013
Published online: February 14, 2014

[1] K. M. Coakley, M. D. McGehee, *Appl. Phys. Lett.* **2003**, *83*, 3380.
[2] B. Ehrler, M. W. B. Wilson, A. Rao, R. H. Friend, N. C. Greenham, *Nano Lett.* **2012**, *12*, 1053–1057.
[3] S. D. Oosterhout, M. M. Wienk, S. S. van Bavel, R. Thiedmann, L. J. A. Koster, J. Gilot, J. Loos, V. Schmidt, R. A. Janssen, *Nat. Mater.* **2009**, *8*, 818–824.
[4] Y. C. Huang, J. H. Hsu, Y. C. Liao, W. C. Yen, S.S. Li, S. T. Lin, C. W. Chen, W. F. Su, *J. Mater. Chem.* **2011**, *21*, 4450.
[5] W. Ma, C. Yang, X. Gong, K. Lee, A. J. Heeger, *Adv. Funct. Mater.* **2005**, *15*, 1617–1622.
[6] E. V Canesi, M. Binda, A. Abate, S. Guarnera, L. Moretti, V. D'Innocenzo, R. Sai Santosh Kumar, C. Bertarelli, A. Abrusci, H. Snaith, A. Calloni, A. Brambilla, F. Ciccacci, S. Aghion, F. Moia, R. Ferragut, C. Melis, G. Malloci, A. Mattoni, G. Lanzani, A. Petrozza, *Energy Environ. Sci.* **2012**, *5*, 9068–9076.
[7] N. Bansal, L. X. Reynolds, A. MacLachlan, T. Lutz, R. S. Ashraf, W. Zhang, C. B. Nielsen, I. McCulloch, D. G. Rebois, T. Kirchartz, M. S. Hill, K. C. Molloy, J. Nelson, S. A. Haque, *Sci. Rep.* **2013**, *3*, 1–8.
[8] M. T. Lloyd, R. P. Prasankumar, M. B. Sinclair, A. C. Mayer, D. C. Olson, J. W. P. Hsu, *J. Mater. Chem.* **2009**, *19*, 4609.
[9] B. Conings, L. Baeten, H.-G. Boyen, D. Spoltore, J. D'Haen, L. Grieten, P. Wagner, M. K. Van Bael, J. V. Manca, *J. Phys. Chem. C* **2011**, *115*, 16695–16700.
[10] C. Goh, S. R. Scully, M. D. McGehee, *J. Appl. Phys.* **2007**, *101*, 114503.
[11] M. Meister, J. J. Amsden, I. A. Howard, I. Park, C. Lee, D. Y. Yoon, F. Laquai, *J. Phys. Chem. Lett.* **2012**, *3*, 2665–2670.
[12] F. C. Spano, *J. Chem. Phys.* **2005**, *122*, 234701.
[13] J. Clark, C. Silva, R. Friend, F. Spano, *Phys. Rev. Lett.* **2007**, *98*, 206406.
[14] G. Malloci, M. Binda, A. Petrozza, A. Mattoni, *J. Phys. Chem. C* **2013**, *117*, 13894–13901.
[15] E. Burstein, *Phys. Rev.* **1953**, 632.
[16] B. Enright, D. Fitzmaurice, *J. Phys. Chem.* **1996**, *100*, 1027–1035.
[17] G. Boschloo, D. Fitzmaurice, *J. Phys. Chem. B* **1999**, *103*, 2228–2231.
[18] G. Redmond, A. O. Keeffe, C. Burgess, C. Machale, D. Fitzmaurice, *J. Phys. Chem.* **1993**, 11081–11086.
[19] G. Lakhwani, R. F. H. Roijmans, A. J. Kronemeijer, J. Gilot, R. A. Janssen, S. C. J. Meskers, *J. Phys. Chem. C* **2010**, *114*, 14804–14810.
[20] J. A. Faucheaux, P. K. Jain, *J. Phys. Chem. C* **2013**, *4*, 3024–3030.
[21] H. Y. Xu, Y. C. Liu, R. Mu, C. L. Shao, Y. M. Lu, D. Z. Shen, X. W. Fan, *Appl. Phys. Lett.* **2005**, *86*, 123107.
[22] A. Schleife, C. Rödl, F. Fuchs, K. Hannewald, F. Bechstedt, *Phys. Rev. Lett.* **2011**, *107*, 236405.
[23] G. Mahan, *Phys. Rev.* **1967**, *153*, 882–889.
[24] P. Kamat, N. Dimitrijevic, A. Nozik, *J. Phys. Chem.* **1989**, *93*, 2873–2875.
[25] U. Ozgur, Y. I. Alivov, C. Liu, A. Teke, M. A. Reshchikov, S. Dogan, V. Avrutin, S.-J. Cho, H. Morkoc, *J. Appl. Phys.* **2005**, *98*, 041301.
[26] A. Calloni, A. Brambilla, G. Berti, G. Bussetti, E. V Canesi, M. Binda, A. Petrozza, M. Finazzi, F. Ciccacci, L. Duò, *Langmuir* **2013**, *29*, 8302–8310.
[27] A. Ruseckas, P. E. Shaw, I. D. W. Samuel, *Dalt. Trans.* **2009**, *45*, 10040–10043.
[28] S. Singh, B. Pandit, T. Basel, S. Li, D. Laird, Z. Vardeny, *Phys. Rev. B* **2012**, *85*, 205206.
[29] G. D'Avino, S. Mothy, L. Muccioli, C. Zannoni, L. Wang, J. Cornil, D. Beljonne, F. Castet, *J. Phys. Chem. C* **2013**, *117*, 12981–12990.
[30] A. R. S. Kandada, G. Grancini, A. Petrozza, S. Perissinotto, D. Fazzi, S. S. K. Raavi, G. Lanzani, *Sci. Rep.* **2013**, *3*, 2073.
[31] Y. Sun, J. H. Seo, C. J. Takacs, J. Seifter, A. J. Heeger, *Adv. Mater.* **2011**, *23*, 1679–83.